# Quantifying the Cenozoic marine diatom deposition history: links to the C and Si cycles

Johan Renaudie[1]

[1]Museum für Naturkunde, Leibniz-Institut für Evolutions- und Biodiversitätsforschung, Berlin, Germany.

*Correspondence to:* Johan Renaudie (johan.renaudie@mfn-berlin.de)

**Abstract.** Marine planktonic diatoms are, today, among the world's main primary producers as well as the main organic carbon exporter to the deep-sea despite the fact that they were a very minor component of the plankton at the beginning of the Cenozoic. They are also the main silica exporter to the deep-sea, thus balancing global chemical weathering. This study reviews their global Cenozoic depositional pattern in order to understand the modality and the context of their rise to dominance, but also to understand how diatom evolution affected the Cenozoic functioning of the ocean's biological pump. After two short-lived major abundance peaks near the Eocene/Oligocene boundary and in the late Oligocene, diatom abundance in sediments shifted in the mid-Miocene to globally higher values which have largely persisted to the modern day. These quantitative findings provide support for the hypothesis according to which diatoms, through their ecological role in the ocean's biological carbon pump, have contributed to the Cenozoic changes in atmospheric carbon dioxide pressure and consequently to changes in the global climate state. Additionally, correlations between diatom abundance peaks and shifts in seawater strontium and osmium isotopic composition hint at a strong control of the silicate weathering on diatom deposition.

## 1 Introduction

The Cenozoic history of oceanic silica deposition is a key piece of information in understanding the Cenozoic evolution of global weathering, ocean productivity and carbon accumulation, both as atmospheric $p_{CO_2}$ and as sedimentary $C_{org}$. Oceanic silica deposition, on scales of millions of years or more, is the main sink for silica released by continental and ocean crust weathering (Tréguer et al., 1995). Because dissolved ocean silica has a short residence time (Heath, 1974), marine opal deposition can be viewed as a proxy for the intensity of silicate weathering and cycling over time. In modern oceans, silica residence times are short in part because most of the silica is rapidly removed from ocean waters and sequestered as opaline sedimentary silica by marine planktonic diatoms (Heath, 1974; Nelson et al., 1995; Tréguer and Pondaven, 2000). This diatom production is also responsible for nearly half of ocean productivity (and approximately one quarter of global primary production), and is the single largest component of the ocean biologic carbon pump (Smetacek, 1999; Ragueneau et al., 2000, 2006). The history of silica deposition in Cenozoic oceans can thus also provide important insights into the history of the ocean's carbon pump (Smetacek, 1999; Cermeño et al., 2008). Marine planktonic diatoms, as the main driver of this process, are known to have themselves diversified dramatically over the Cenozoic (Lazarus et al., 2014), originating from primarily coastal, benthic ancestors in the late Cretaceous (Fenner, 1985). Many authors, in the absence of detailed records of Cenozoic opal deposition,

have used this diversity history of diatoms as a proxy for the intensity of opal export and deposition (Falkowski et al., 2004; Katz et al., 2007; Lazarus et al., 2014). Although diatom diversity and productivity are probably linked (Lazarus et al., 2014), the control of diatom diversity on the Cenozoic oceanic silica cycle and deposition of marine biogenic opal is still largely unexamined, as is the balance over the Cenozoic between diatom derived biogenic opal and that deposited by other organisms (mostly polycystine radiolarians and hexactinellid sponges).

Diatom primary productivity in the water column is usually limited by silicic acid availability in surface waters (Leynaert et al., 2001; Yool and Tyrrell, 2003; Brzezinski et al., 2011). It is concentrated in the modern ocean in several discrete areas of localised, wind-driven or regional upwelling of intermediate, more silica-rich ocean waters with at least seasonally weak water density stratification (Lisitzin, 1972; Heath, 1974; Garcia et al., 2010). Silica in the ocean is undersaturated at all depths (Siever, 1957; Garcia et al., 2010) (see also Fig. 1) and preservation as sediment only occurs when the export flux exceeds the dissolution rate in the water column and the upper layers of sediment (DeMaster, 2002; Tréguer and De La Rocha, 2013). Dissolution rates in the water column are in turn affected by patterns of deep-water flow between basin and deep ocean dissolved silica concentration (Berger, 1970). Accumulation of opal in marine sediments thus occurs only in a fairly complex, geographically patchy global pattern. It deposits primarily in the Southern Ocean belt, followed by the North Pacific and the Eastern Indian Ocean, as well as continental margin upwelling areas, and to a much lesser extent estuarine environment (Lisitzin, 1972; DeMaster, 1981) (Fig. 2). This makes reconstructing past global opal deposition more challenging than for carbonate, the other main biogenic mineral phase deposited in ocean sediments, since the saturation of water in respect to it depends primarily on pressure (i. e. depth) and is therefore largely constant across ocean basins: its deposition history can be thus reconstructed by a fairly small number of depth transects of sediment sections over time (Van Andel, 1975; Berger, 1978).

Although abiotic removal of silica from the ocean is thought to have dominated until the late Cambrian (Maliva et al., 2005), since then, the oceanic silica cycle output have been almost exclusively biologically controlled (Maliva et al., 1989): prior to the Cretaceous, it seems to have been dominated by sponge spicules and radiolarians, and since then, by diatoms and radiolarians. Existing studies on the Cenozoic history of opal deposition (Brewster, 1980; Miskell et al., 1985; Baldauf and Barron, 1990; Cortese et al., 2004; Muttoni and Kent, 2007) are few, mostly qualitative, substantially limited in the data or methods used, and, for full Cenozoic scale, more than two decades old, thereby missing a great deal of new data from later drilling by ODP and IODP. A new synthesis is appropriate, and is the goal of this paper.

## 2   Material and Methods

The analyzed dataset is based on all smear slide descriptions published in the Initial Reports of the Deep-Sea Drilling Program (DSDP), Legs 1 to 96, Ocean Drilling Project (ODP), Legs 101 to 129 (available from National Geophysical Data Center, 2000, 2001) and Legs 178 to 201 (available from the Janus Database; Mithal and Becker, 2006), and Integrated Ocean Drilling Program (IODP), Legs 306 to 308 (also available from the Janus database). Legs 130 to 177 Initial Reports only contain semi-quantitative descriptions of smear slide components, and therefore were not used in this study. The omission of Legs 130-177 data does not seriously bias the results, although some smaller regions such as the Benguela Upwelling System, primarily

cored by Leg 175, are poorly represented in this analysis. The dataset consists, for each sample, of an estimate of the relative abundance of each element seen on the smear slide (microfossil or mineral). In total, the dataset contains 96669 samples, but only the 31136 samples for which a numerical age could be estimated with reasonable accuracy have been kept for the analysis. Out of the dated samples, 10832 contained diatoms, 9744 contained radiolarians, 3568 silicoflagellates and 4068 slides con-

5    tained sponge spicules. The use of smear slides description data comes with many caveats: the non-uniform preparation of the slides, the varying taxonomical expertise of the sedimentologists describing the slides, the difficulty to recognize most diatom specimens at lower magnification or in carbonate-rich sediments are among the issues that should hamper our ability to recover correctly any signal from this dataset. In practice however both spatial and temporal trends in smear slides and quantitative opal measurements tend to be very similar (see Fig. 2 and Supplementary Figure 2), making smear slides description data a

10    reasonable proxy for microfossil abundance in sediments. Smear slides however do not provide estimates of chert abundance, and thus systematically underestimate opal in sections where significant silica diagenesis has occurred. This, however, only affects significantly the older Paleogene record, as chert abundance has been shown to decline significantly after accoustic horizon $A_c$ (i. e. 45 Ma, Muttoni and Kent, 2007). The sources of the age models are detailed in Supplementary Table S1. All ages are given on the Gradstein et al. (2012) geomagnetic polarity time-scale. For the computations leading to Fig. 3 and

15    5, the data were binned into 1 Myr time intervals. The reason behind this choice is twofold: high-resolution studies (Cortese et al., 2004) revealed patterns at the scale of 1 Myr; and, although the amount of data is sufficient when using 1 Myr steps to allow statistically significant results (see confidence intervals on Figs. 3 and 5) in most timebins, it is not the case when using narrower steps such as 0.5 Myr. Median relative abundance were calculated, as well as the interquartile range (i. e. from 1st to 3rd quartile; Tukey, 1977) and the 95% confidence interval on the median (McGill et al., 1978) for each 1 Myr time-bin.

20    The spatial pattern of the diatom distribution in the DSDP and ODP dated sediments is shown on Fig. 4 for each subepoch (from middle Eocene to Pleistocene). On those maps, the geographical pattern is interpolated between each samples available in said sub-epoch using Ordinary Kriging, based on an exponential semi-variogram model (Matheron, 1963; Cressie, 1993). The paleocoordinates of each DSDP and ODP sites, as well as the past continental configurations, were reconstructed using rotation poles, plates and coastlines datasets from the Earthbyte project (Müller et al., 2008). Paleogeographic reconstructions were

25    made using GPlates 1.4.0 (Boyden et al., 2011) and the interpolation and final maps were produced programmatically using R 3.2.3 (R Core Team, 2015). Similarly, the spatial pattern of siliceous microfossils (diatoms, radiolarians, silicoflagellates and sponge spicules) in the Pleistocene was produced using the same method and is shown on Fig. 2, for comparison with the spatial pattern of biogenic opal measured in surface sediments, reconstructed from Archer (1996), and the spatial pattern of silicic acid at the bottom of the photic zone, reconstructed from Garcia et al. (2010).

30    ## 3   Results

While radiolarians were blooming from ca. 50 Ma (early Eocene) until the earliest late Eocene (McGowran, 1989; Muttoni and Kent, 2007) (Fig. 3), the proportion of samples containing diatoms prior to 45 Ma (Middle Eocene) is too low to yield a reliable global median abundance. From that point on, however, diatom-bearing samples are numerous and geographically

widespread, as they are found at all latitude and in all ocean basins (see Fig. 4) (Miskell et al., 1985; Baldauf and Barron, 1990; Barron et al., 2015). At the transition between the late Eocene and the early Oligocene (from ca. 35 to 31 Ma), diatom abundance peaked (Fig. 3) in the high latitudes (Fig. 4), with a main deposition locus in the south Atlantic (Salamy and Zachos, 1999; Diekmann et al., 2004). Six Myr after this event, a smaller abundance peak occured in the late Oligocene (between 26 and 24 Ma; Fig. 3). Once again, this event is more strongly marked in the southern high latitude, with, for the first time in the Cenozoic, an higher abundance in all three sectors of the Southern Ocean (Fig. 4), hinting at a circum-Antarctic accumulation belt. During the early Miocene, diatom abundance in sediments was somewhat lower, with, for the first time, some loci of higher deposition in the middle latitude (Fig. 4), loci that expanded during the middle Miocene: this is most probably linked to the beginning of the coastal mid-latitude upwelling zones such as the Canary and the Californian upwelling seen on the early Miocene maps. At ca. 15 Ma, the abundance pattern rises again progressively until it reaches a plateau of relatively high abundance (Fig. 3). The middle Miocene is also marked by a geographical change in the distribution of diatom abundance: until then, high abundances are limited to the Atlantic basin (and the Southern Ocean) whereas, starting from the mid-Miocene, the northern Pacific Ocean, followed later by the western Pacific and the eastern Indian Ocean dominate (Fig. 4). Direct records of biogenic opal for the Neogene (Keller and Barron, 1983; Baldauf and Barron, 1990; Cortese et al., 2004) confirm this shift in opal deposition loci from the Atlantic (with noticeably a collapse of North Atlantic opal) to the Pacific. Additionally, as was noted before (Kennett, 1978; Brewster, 1980), siliceous sedimentation becomes predominant in the Southern Ocean, thus establishing the modern Southern Ocean diatom belt (Burckle and Cirilli, 1987) (Fig. 4). The abundance plateau initiated during the middle Miocene event is more or less sustained until the Pleistocene, although the median relative abundance of diatoms seems to drop somewhat between 3 and 2 Ma (Fig. 3), yet still remaining above pre-15 Ma level. This decline mainly affected the low to mid-latitudes, which might indicate a shrinking of the diatom polar-centered hotspots (Fig. 4) and reduced abundance in the North Pacific. By contrast, the median abundance in the Indian Ocean rose significantly (Fig. 4).

The spatial pattern observed for the Pleistocene for cumulated siliceous microfossils (Fig. 2) is largely coherent not only with the modern distribution of biogenic silica in sediments (Lisitzin, 1972; Archer, 1996) but also with the modern distribution of the silicic acid in the upper 200m layer of the ocean, i. e. the euphotic zone (Fig. 2) (Garcia et al., 2010): Spearman's rank correlation coefficient (Spearman, 1904) on paired cells at $1°$ resolution yield $\rho = 0.464$ ($p < 2.2 \times 10^{-16}$) when comparing the smear slide data with Archer (1996) interpolated map, and $\rho = 0.399$ ($p < 2.2 \times 10^{-16}$) when compared with the silicic acid at 200m. Comparison with Fig. 4 shows that the main loci of diatom deposition in both the current analysis results for the Pleistocene and the reference datasets are the Southern Ocean, followed by the North Pacific and the eastern Indian Ocean while radiolarians add an opal deposition locus in the Pacific equatorial belt. The lower abundance of diatoms in this particular region could be a combined effect of the dissolution rate that affects diatoms more than radiolarians (e. g. Lisitzin, 1972) and a difference in silica concentration between the top and the bottom of the photic zone (Garcia et al., 2010), as radiolarians are more abundant at the bottom of the photic zone (e. g. Boltovskoy et al., 2010). These comparisons also show the adequacy of the method to delimit patterns of biogenic opal deposition, at least on a broad scale, both temporally and spatially.

The observed early Oligocene maxima in global diatom relative abundance is broadly coeval (Fig. 5) with an acceleration of the radiogenic strontium input (Barrera et al., 1991; Mead and Hodell, 1995; Zachos et al., 1999), with an abrupt shift

in the $\delta^{18}$O signal that indicates an abrupt cooling (Zachos et al., 2001, 2008), and a decrease of atmospheric $CO_2$ (Pagani et al., 2005). In addition to the strontium regime change, an abrupt drop in $^{187}$Os/$^{188}$Os before the event (at 34.5 Ma), followed by an equally abrupt recovery at ca. 33.5 Ma, to finally reach a regime of slow increase (from ca. 33.5 to ca. 15 Ma), has also been described (Dalai et al., 2006). Both have been interpreted (Zachos et al., 1999; Dalai et al., 2006) as marks

5   of increased weathering of the Antarctic continent following the early Oligocene glaciation (Oi-1). Similarly, the shift toward higher abundance of diatoms that starts at the beginning of the middle Miocene corresponds, temporally, to a shift in the oxygen isotope record . This cooling trend follows the Mid-Miocene Climatic Optimum (Zachos et al., 2001) and is reflected in the rate of change of the strontium isotope record (Hodell et al., 1991; Hodell and Woodruff, 1994; Ravizza and Zachos, 2003). In addition to the strontium record, the osmium isotope record also underwent a clear break in the early middle Miocene,

10   changing from an Oligocene to Miocene plateau to a rapid late Neogene increase (Peucker-Ehrenbrink et al., 1995). The coupling of those two isotope systems (Sr and Os) have been interpreted as an indication of intense continental weathering, namely of the Himalayas (Peucker-Ehrenbrink et al., 1995).

The shift in diatom relative abundance observed near the Eocene/Oligocene boundary (and well documented in the literature, Baldauf and Barron, 1990; Katz et al., 2004; Kooistra et al., 2007) also coincides with a substantial increase in diatom diversity

15   (Lazarus et al., 2014) as well as an increase in provincialism (Fenner, 1985; Lazarus et al., 2014). Not only does the Southern Atlantic seem to be the main focus of the late Eocene - early Oligocene event, but the Southern Ocean flora is known to have undergone a strong turnover at the Eocene-Oligocene transition (Kennett, 1978; Baldauf, 1992). The mid-Miocene shift in diatom abundance pattern is also associated with a well-documented diatom diversification event (Lazarus et al., 2014) (Fig. 5). Lazarus et al. (2014) showed that the vast majority of the living species of marine diatoms originated from 15 Ma

20   onwards.

## 4   Discussion

Although the diatom depositional history mimics neither the $^{87}$Sr/$^{86}$Sr record nor the $^{187}$Os/$^{188}$Os record, it does appear to respond noticeably to changes in the long-term trends in these parameters (in the earlier Oligocene and the early middle Miocene), suggesting significant control of rates of weathering on Cenozoic diatom abundance: increased weathering resulting

25   in increased silica availability in the world's oceans and thus increased export of silica by diatoms to the sedimentary record. Diatom export is also linked to Cenozoic climate history since both major shifts in weathering rates are temporally correlated to the two largest Cenozoic cooling events: Oi-1 (Zachos et al., 2001) and the middle Miocene climatic transition (Flower and Kennett, 1994). Inferring the direction of causal relationship is difficult here because of the low temporal resolution of Figs 2–5, however silicon isotope ($\delta^{30}$Si) measurements (Egan et al., 2013) on late Eocene - early Oligocene antarctic diatoms

30   and sponges showed that increased diatom productivity (through an increase in silicic acid utilisation) started before the Oi-1 event – the first high values of $\delta^{30}$Si occurring as early as ca. 37 Ma, and increasing until 34.5 Ma, which seem to concur with the increase in diatom abundance seen here as starting in the 36 to 35 Ma time bin.

The largest single fraction of the global Cenozoic signal is from changes in the southern high latitudes (Fig. 4). Diatom accumulated in all sectors of the Southern Ocean as early as the late Oligocene although it did not form a proper diatom accumulation belt before the middle Miocene. A distinct Southern Ocean surface circulation with endemic biotas extends back to the late Eocene (Lazarus et al., 2008). The Antarctic Circumpolar Current (ACC) with its current physical properties (specifically its depth) however may have formed only in the late Oligocene (at ca. 25 Ma Lyle et al., 2007), though there is debate on the subject (Barker and Thomas, 2004). If a late Oligocene formation of the ACC is confirmed, then, considering the timing and the geographical extent of the late Oligocene diatom accumulation event, it is plausible that this new circulation pattern triggered increased opal deposition in the Southern Ocean. The increase of opal deposition seen in the Southern Ocean could also be relative and only reflect a decrease in carbonate deposition, however carbonate microfossil deposition was still fairly abundant well into the Miocene (Lazarus and Caulet, 1993; Renaudie and Lazarus, 2013). The shift of the main diatom deposition locus starting at ca. 15 Ma from the Atlantic to the Pacific oceans (i. e. the event known as the 'silica switch'; Keller and Barron, 1983; Cortese et al., 2004) is one of the main changes in geographic pattern seen in the Cenozoic history of silica deposition. The reasons for this switch have been interpreted by several previous authors (Keller and Barron, 1983; Baldauf and Barron, 1990; Flower and Kennett, 1994; Cortese et al., 2004) as a consequence of the formation of the North Atlantic Deep Water component which suppressed transport and upwelling of Antarctic Bottom Water into the North Atlantic, thus turning the Atlantic Ocean into a 'lagoonal'-type ocean (sensu Berger (1970), i. e. with deep-water outflow) and leading to silica-richer waters in the Pacific and Indian Ocean ('estuarine'-type sensu Berger (1970), i. e. with deep-water inflow).

Past fluctuations of species diversity and links to possible causal factors, e.g climatic or environmental changes, are central themes in paleobiology. Most scenarii invoked to explain such correlations implicitly assume that diversity is strongly correlated to ecologic abundance, even though this correlation is rarely tested. Although there is no strict one-to-one relationship between Cenozoic diatom abundance and diversity (Fig. 5), the primary periods of diversity change and turnover (Cervato and Burckle, 2003; Lazarus et al., 2014) occurred during periods of abundance shifts (the ca. 33 Ma and the ca. 15 Ma events). Only the Late Oligocene abundance maximum does not correspond to any known global diversity increase. This may be explainable by the relatively narrow geographical extent of the event (Fig. 4). There is additionally in the Neogene a strong correlation between the abundance curve presented herein and the diversity curve (Lazarus et al., 2014): the correlation over the last 25 Myr has a Pearson's $r = 0.77$ ($p = 9.8 \times 10^{-6}$); and a Pearson's $r = 0.52$ ($p = 0.009$) when detrended linearly.

Biogenic opal accumulation rates (which in the Cenozoic in most regions corresponds almost exclusively to the diatom accumulation rate (Tréguer and De La Rocha (2013); Fig. 2) are often used as an indicator of paleoproductivity (Hüneke and Henrich, 2011). The studied dataset only gives access to diatom relative abundance in the sediment (not absolute abundance, or accumulation rate) so the variations seen here do not correspond to absolute variations of the paleoproductivity but, at best, to variations of the diatom contribution to the paleoproductivity. However, the diatom contribution to primary production is known to be (today) the dominant exporter of carbon to the deep sea, i. e. this is the main component of the ocean's biological pump (Smetacek, 1999; Cermeño et al., 2008); diatom relative abundance in the sediments should therefore indicate the relative strength of the biological carbon pump versus the contribution of the so-called 'alkalinity pump', that corresponds mainly to the activity of calcareous nannoplankton (Frankignoulle et al., 1994). A comparison of diatom abundance with the $p_{CO_2}$

Cenozoic curve (Beerling and Royer, 2011) (Fig. 5) show that each increase of diatom abundance corresponds to a drop in $p_{CO_2}$: at ca. 33 Ma, ca. 26 Ma and ca. 15 Ma. Higher global diatom relative abundance does seem to be linked with decreased atmospheric $p_{CO_2}$, meaning not only that the diatom relative abundance might indeed be a good proxy for export productivity but also that there is evidence in our results for a diatom-to-climate causal interaction during most of the Cenozoic as has

5   been speculated or modeled before (Tréguer et al., 1995; Pollock, 1997; Lazarus et al., 2014; Falkowski et al., 2004; Katz et al., 2007). The use of 1 Myr time bins is of course still too broad to show directly a cause-and-effect relationship, but the observation of a clear correlation and a coherent model to explain it (i. e. the biological carbon pump) are already strong evidence in favor of such a relationship. The resulting scenarii for each of the two main events observed, should this relationship be correct, would thus be the following: during the mid-Miocene event, the uplift of the Tibetan Plateau caused increased

10  silicate weathering, which in turn favored an increase in diatom abundance in the oceans; consequently, the atmospheric $p_{CO_2}$ decreased which, together with the various feedback mechanisms (such as larger amount of continental relief available for chemical erosion, which consumes atmospheric $p_{CO_2}$, or the high topography which is responsible for higher rainfall linked to the Asian monsoon) resulting directly from the Himalayan orogenesis (Raymo and Ruddiman, 1992), induced a global cooling. The Eocene-Oligocene transition event and interactions between $p_{CO_2}$ and polar circulation have been extensively discussed

15  in the literature, but, if the timing of events implied by Egan et al. (2013) is correct, the role of diatoms is to provide the $p_{CO_2}$ forcing that results in Antarctic continental glaciation: the opening of the Drake Passage allows a surface circum-Antarctic current to circulate, thus bringing more nutrients to the southern Atlantic diatom communities, increased diatom productivity, long-term carbon export into marine sediments, drawdown of atmospheric $p_{CO_2}$ and a cooling event. This cooling, together with the thermic isolation of the Antarctic continent by the proto-ACC, results in the formation of the East Antarctic Ice Sheet;

20  the resulting weathering of the Antarctic continent by this ice-sheet creating finally a positive feedback through an even higher input of silica into the oceans and higher diatom abundance.

When comparing the variations of total biogenic opal (i. e. diatoms, radiolarians, silicoflagellates and sponge spicules) in deep-sea sediments during the Cenozoic, with variations in diatom and radiolarian abundance in sediments (Fig. 3), one striking feature is that, prior to the Eocene-Oligocene boundary, the total biogenic opal variations is almost exclusively due to

25  radiolarians but that from the Oligocene onwards, it is the diatom which accounts for most of the biogenic opal variation. Harper and Knoll (1975) suggested the possibility of a competition – on a geological time scale – between diatoms and radiolarians for dissolved silica in sea water. Later, Lazarus et al. (2009) confirmed the reduction in radiolarian silica use, and showed that it primarily resulted from a marked trend in tropical radiolarian shell thinning around the Eocene-Oligocene transition, with little change seen in polar regions. The authors argued that the tropical restriction of this morphologic trend was evidence for

30  strong, diatom-dominated silica removal from low latitude surface waters, beginning in strongly stratified post-Eocene oceans. They were not able to compare their radiolarian data to any direct measures of opal export, but showed that the Cenozoic pattern of decreasing radiolarian silica use matched that of increasing diatom diversity. Similarly, a model-based approach by Cermeño et al. (2015) confirmed the impact of an increased silica flux on the dominance of diatoms over radiolarians, through competition. This take-over of the biological marine Si cycle by diatoms at this time is here confirmed.

The deposition of biogenic opal is the only output from the marine Si cycle (Tréguer et al., 1995), while continental weathering is the dominant input to this system, with only smaller contributions from hydrothermal activity, aeolian dust and seafloor weathering. In theory, biogenic opal deposition should therefore compensate global silicate weathering on a geological timescale. The curve presented here (Fig. 3) shows only relative abundances of biogenic silica-bearing microfossils in sediments, not accumulation rates; however, unless there have been systematic changes in average global total biogenic sediment accumulation rates on Myr scales over the Cenozoic, the globally averaged relative abundance data presented here should largely track variations in global opal accumulation rates, and could therefore, in theory, be used as a proxy for Cenozoic silica weathering rate.

## 5   Summary and Conclusions

Diatoms have increased in abundance over the Cenozoic, with two main abundance events, one at the Eocene-Oligocene transition, another during the Mid-Miocene. These events correlate with shifts in seawater strontium and osmium isotope composition, hinting at a strong control of the weathering on diatom abundance. Paleoceanographic and paleoclimatic events such as the onset of the Antarctic Circumpolar current and the establishment of a permanent Northern Hemisphere Ice Sheet might have also exerted control on local events of diatom abundance (respectively the Southern Ocean late Oligocene maxima and the collapse of the North Pacific diatom deposition in the late Pliocene).

Beyond the simple abundance shift, the Mid-Miocene event also witnessed a complete spatial reorganization of the diatom deposition loci, switching from the Atlantic to the Pacific and Indian basins. It is also during this event that the modern Southern Ocean diatom accumulation belt formed.

The findings presented here also provide support for the scenario in which diatoms, through their ecological role in the ocean's carbon pump, might be responsible at least in part for Cenozoic changes in atmospheric carbon dioxide pressure and therefore changes in global climate state. The quality and spatiotemporal coverage of the studied data is not yet sufficient however to determine the sequence of changes, in diatom abundance versus climate changes, and therefore causality cannot be determined with any statistical certainty. Similarly, the role of diatoms in the Si cycle is shown here to be dominant since the Eocene-Oligocene transition, hinting that the abundance of diatoms in sediments might echo quantitatively the amount of global chemical weathering.

*Author contributions.*   J.R. conceived and conducted the study, analyzed the results and wrote the manuscript.

*Competing interests.*   The author declare that he has no conflict of interest.

*Acknowledgements.*   The author is currently supported financially by a DFG (German science foundation) grant RE 3470/1-3. The author would like to thank D. Lazarus for his support during this study; J. Witkowski and M. Schobben for constructive feedback on previous

versions of this manuscript; Reed Sherer and two anonymous reviewers for their thorough reviews; Kristina Pascher and Zuzia Stroynowski for additional comments on this manuscript.

# References

Archer, D. E.: An atlas of the distribution of calcium carbonate in sediments of the deep sea, Global Biogeochemical Cycles, 10, 159–174, 1996.

Baldauf, J.: Middle Eocene through early Miocene diatom floral turnover, in: Eocene-Oligocene climatic and biotic evolution, edited by Prothero, D. and Berggren, W., pp. 310–326, Princeton University Press, Princeton, NJ, 1992.

Baldauf, J. and Barron, J.: Evolution of biosiliceous sedimentation patterns—Eocene through Quaternary: paleoceanographic response to polar cooling, in: Geological History of the Polar Oceans: Arctic Versus Antarctic, edited by U, B. and J, T., vol. 308 of *NATO ASI Series C*, pp. 575–607, Springer, 1990.

Barker, P. and Thomas, E.: Origin, signature and palaeoclimatic influence of the Antarctic Circumpolar Current, Earth-Science Reviews, 66, 143–162, 2004.

Barrera, E., Barron, J., and Halliday, A.: Strontium isotope stratigraphy of the Oligocene-lower Miocene section at Site 744, southern Indian Ocean, in: Proceedings of the Ocean Drilling Program, Scientific Results, edited by Barron, J. et al., vol. 119, pp. 731–738, Ocean Drilling Program, College Station, TX, 1991.

Barron, J. A., Stickley, C. E., and Bukry, D.: Paleoceanographic, and paleoclimatic constraints on the global Eocene diatom and silicoflagellate record, Palaeogeography, Palaeoclimatology, Palaeoecology, 422, 85–100, 2015.

Beerling, D. J. and Royer, D. L.: Convergent cenozoic $CO_2$ history, Nature Geoscience, 4, 418–420, 2011.

Berger, W. H.: Biogenous deep-sea sediments: fractionation by deep-sea circulation, Geological Society of America Bulletin, 81, 1385–1402, 1970.

Berger, W. H.: Sedimentation of deep-sea carbonate; maps and models of variations and fluctuations, The Journal of Foraminiferal Research, 8, 286–302, 1978.

Boltovskoy, D., Kling, S. A., Takahashi, K., and Bjørklund, K.: World atlas of distribution of recent Polycystina (Radiolaria), Palaeontologia Electronica, 13, 230, 2010.

Boyden, J. A., Müller, R. D., Gurnis, M., Torsvik, T. H., Clark, J. A., Turner, M., Ivey-Law, H., Watson, R. J., and Cannon, J. S.: Next-generation plate-tectonic reconstructions using GPlates, in: Geoinformatics: cyberinfrastructure for the solid earth sciences, edited by Keller, G. and Baru, C., pp. 95–114, Cambridge University Press, Cambridge, UK, 2011.

Brewster, N. A.: Cenozoic biogenic silica sedimentation in the Antarctic Ocean, Geological Society of America Bulletin, 91, 337–347, 1980.

Brzezinski, M. A., Baines, S. B., Balch, W. M., Beucher, C. P., Chai, F., Dugdale, R. C., Krause, J. W., Landry, M. R., Marchi, A., Measures, C. I., Nelson, D. M., Parker, A. E., Poulton, A. J., Selph, K. E., Strutton, P. G., Taylor, A. G., and Twining, B. S.: Co-limitation of diatoms by iron and silicic acid in the equatorial Pacific, Deep Sea Research Part II: Topical Studies in Oceanography, 58, 493–511, 2011.

Burckle, L. H. and Cirilli, J.: Origin of diatom ooze belt in the Southern Ocean: Implications for late Quaternary paleoceanography, Micropaleontology, pp. 82–86, 1987.

Cermeño, P., Dutkiewicz, S., Harris, R. P., Follows, M., Schofield, O., and Falkowski, P. G.: The role of nutricline depth in regulating the ocean carbon cycle, Proceedings of the National Academy of Sciences, 105, 20 344–20 349, 2008.

Cermeño, P., Falkowski, P. G., Romero, O. E., Schaller, M. F., and Vallina, S. M.: Continental erosion and the Cenozoic rise of marine diatoms, Proceedings of the National Academy of Sciences, 112, 4239–4244, 2015.

Cervato, C. and Burckle, L.: Pattern of first and last appearance in diatoms: oceanic circulation and the position of polar fronts during the Cenozoic, Paleoceanography, 18, 2003.

Cleveland, W. S., Grosse, E., and Shyu, W. M.: Local regression models, in: Statistical models in S, edited by Chambers, J. M. and Hastie, T., pp. 309–376, Chapman and Hall, New York, 1992.

Cortese, G., Gersonde, R., Hillenbrand, C.-D., and Kuhn, G.: Opal sedimentation shifts in the World Ocean over the last 15 Myr, Earth and Planetary Science Letters, 224, 509–527, 2004.

5   Cressie, N.: Statistics for spatial data, John Wiley & Sons, 1993.

Dalai, T. K., Ravizza, G. E., and Peucker-Ehrenbrink, B.: The Late Eocene $^{187}$Os/$^{188}$Os excursion: chemostratigraphy, cosmic dust flux and the early Oligocene glaciation, Earth and Planetary Science Letters, 241, 477–492, 2006.

DeMaster, D. J.: The supply and accumulation of silica in the marine environment, Geochimica et Cosmochimica acta, 45, 1715–1732, 1981.

DeMaster, D. J.: The accumulation and cycling of biogenic silica in the Southern Ocean: revisiting the marine silica budget, Deep Sea
10      Research Part II: Topical Studies in Oceanography, 49, 3155–3167, 2002.

Diekmann, B., Kuhn, G., Gersonde, R., and Mackensen, A.: Middle Eocene to early Miocene environmental changes in the sub-Antarctic Southern Ocean: evidence from biogenic and terrigenous depositional patterns at ODP Site 1090, Global and Planetary Change, 40, 295–313, 2004.

Egan, K. E., Rickaby, R. E., Hendry, K. R., and Halliday, A. N.: Opening the gateways for diatoms primes Earth for Antarctic glaciation,
15      Earth and Planetary Science Letters, 375, 34–43, 2013.

Falkowski, P. G., Schofield, O., Katz, M. E., Van de Schootbrugge, B., and Knoll, A. H.: Why is the land green and the ocean red?, in: Coccolithophores: from molecular processes to global impact, edited by Thierstein, H. and Young, J., pp. 429–453, Springer, 2004.

Fenner, J.: Late Cretaceous to Oligocene planktic diatoms, in: Plankton stratigraphy, edited by Bolli, B., Saunders, J., and Perch-Nielsen, K., pp. 713–762, Cambridge University Press, Cambridge, UK, 1985.

20   Flower, B. P. and Kennett, J. P.: The middle Miocene climatic transition: East Antarctic ice sheet development, deep ocean circulation and global carbon cycling, Palaeogeography, palaeoclimatology, palaeoecology, 108, 537–555, 1994.

Frankignoulle, M., Canon, C., and Gattuso, J.-P.: Marine calcification as a source of carbon dioxide: Positive feedback of increasing atmospheric $CO_2$, Limnology and Oceanography, 39, 458–462, 1994.

Garcia, H., Locarnini, R., Boyer, T., Antonov, J., Zweng, M., Baranova, O., and Johnson, D.: World Ocean Atlas 2009, Volume 4: Nutrients
25      (phosphate, nitrate, silicate), in: NOAA Atlas NESDIS, edited by Levitus, S., p. 398pp, U.S. Government Printing Office, Washington, DC, 2010.

Gradstein, F. M., Ogg, J. G., Schmitz, M. D., and Ogg, G. M.: The Geologic Time Scale, Elsevier, Amsterdam, 2012.

Harper, H. E. and Knoll, A. H.: Silica, diatoms, and Cenozoic radiolarian evolution, Geology, 3, 175–177, 1975.

Heath, G. R.: Dissolved Silica and Deep-Sea Sediments, in: Studies in Paleo-Oceanography, vol. 20 of *SEPM Special Publications*, pp.
30      77–93, SEPM Society for Sedimentary Geology, 1974.

Hodell, D. A. and Woodruff, F.: Variations in the strontium isotopic ratio of seawater during the Miocene: Stratigraphic and geochemical implications, Paleoceanography, 9, 405–426, 1994.

Hodell, D. A., Mueller, P. A., and Garrido, J. R.: Variations in the strontium isotopic composition of seawater during the Neogene, Geology, 19, 24–27, 1991.

35   Hüneke, H. and Henrich, R.: Pelagic sedimentation in modern and ancient oceans, in: Deep-sea Sediments, edited by Hüneke, H. and Mulder, T., vol. 63 of *Developments in sedimentology*, Elsevier, Amsterdam, 2011.

Katz, M. E., Finkel, Z. V., Grzebyk, D., Knoll, A. H., and Falkowski, P. G.: Evolutionary trajectories and biogeochemical impacts of marine eukaryotic phytoplankton, Annual Review of Ecology, Evolution, and Systematics, pp. 523–556, 2004.

Katz, M. E., Fennel, K., and Falkowski, P. G.: Geochemical and biological consequences of phytoplankton evolution, in: Evolution of Primary Production in the Sea, edited by Falkowski, P. and Knoll, A., pp. 405–430, Elsevier, Amsterdam, 2007.

Keller, G. and Barron, J. A.: Paleoceanographic implications of Miocene deep-sea hiatuses, Geological Society of America Bulletin, 94, 590–613, 1983.

Kennett, J.: The development of planktonic biogeography in the Southern Ocean during the Cenozoic, Marine Micropaleontology, 3, 301–345, 1978.

Kooistra, W., Gersonde, R., Medlin, L. K., and Mann, D. G.: The origin and evolution of the diatoms: their adaptation to a planktonic existence, in: Evolution of primary producers in the sea, edited by Falkowski, P. and Knoll, A., pp. 207–249, Academic Press Inc, Burlington, MA, 2007.

Lazarus, D. and Caulet, J.: Cenozoic Southern Ocean reconstructions from sedimentologic, radiolarian, and other microfossil data, in: The Antarctic paleoenvironment: A perspective on global change., edited by Kennett, J. P. and Warmke, D. A., vol. 60 of *Antarctic Research Series*, pp. 145–174, American Geophysical Union, 1993.

Lazarus, D., Hollis, C., and Apel, M.: Patterns of opal and radiolarian change in the Antarctic mid-Paleogene: Clues to the origin of the Southern Ocean, Micropaleontology, pp. 41–48, 2008.

Lazarus, D., Barron, J., Renaudie, J., Diver, P., and Türke, A.: Cenozoic Planktonic Marine Diatom Diversity and Correlation to Climate Change, PLoS ONE, 9, e84 857, 2014.

Lazarus, D. B., Kotrc, B., Wulf, G., and Schmidt, D. N.: Radiolarians decreased silicification as an evolutionary response to reduced Cenozoic ocean silica availability, Proceedings of the National Academy of Sciences, 106, 9333–9338, 2009.

Leynaert, A., Tréguer, P., Lancelot, C., and Rodier, M.: Silicon limitation of biogenic silica production in the Equatorial Pacific, Deep Sea Research Part I: Oceanographic Research Papers, 48, 639–660, 2001.

Lisitzin, A. P.: Sedimentation in the World Ocean, vol. 17 of *SEPM Special Publications*, SEPM Society for Sedimentary Geology, 1972.

Lyle, M., Gibbs, S., Moore, T. C., and Rea, D. K.: Late Oligocene initiation of the Antarctic circumpolar current: evidence from the South Pacific, Geology, 35, 691–694, 2007.

Maliva, R. G., Knoll, A. H., and Siever, R.: Secular change in chert distribution: a reflection of evolving biological participation in the silica cycle, Palaios, pp. 519–532, 1989.

Maliva, R. G., Knoll, A. H., and Simonson, B. M.: Secular change in the Precambrian silica cycle: insights from chert petrology, Geological Society of America Bulletin, 117, 835–845, 2005.

Matheron, G.: Principles of geostatistics, Economic geology, 58, 1246–1266, 1963.

McGill, R., Tukey, J. W., and Larsen, W. A.: Variations of box plots, The American Statistician, 32, 12–16, 1978.

McGowran, B.: Silica burp in the Eocene ocean, Geology, 17, 857–860, 1989.

Mead, G. A. and Hodell, D. A.: Controls on the $^{87}Sr/^{86}Sr$ composition of seawater from the middle Eocene to Oligocene: Hole 689B, Maud Rise, Antarctica, Paleoceanography, 10, 327–346, 1995.

Miskell, K., Brass, G., and Harrison, C.: Global Patterns in Opal Deposition from Late Cretaceous Late Miocene, AAPG Bulletin, 69, 996–1012, 1985.

Mithal, R. and Becker, D. G.: The Janus database: providing worldwide access to ODP and IODP data, Geological Society, London, Special Publications, 267, 253–259, 2006.

Müller, R. D., Sdrolias, M., Gaina, C., and Roest, W. R.: Age, spreading rates, and spreading asymmetry of the world's ocean crust, Geochemistry, Geophysics, Geosystems, 9, 2008.

Muttoni, G. and Kent, D. V.: Widespread formation of cherts during the early Eocene climate optimum, Palaeogeography, Palaeoclimatology, Palaeoecology, 253, 348–362, 2007.

National Geophysical Data Center: Core Data from the Deep Sea Drilling Project Legs 1-96. World Data Center for Marine Geology & Geophysics, Seafloor Series, 1, http://www.ngdc.noaa.gov/mgg/fliers/00mgg03.html, 2000.

5    National Geophysical Data Center: Core Data from the Deep Sea Drilling Project Legs 101-129. World Data Center for Marine Geology & Geophysics, Seafloor Series, 2, http://www.ngdc.noaa.gov/mgg/geology/odp/start.htm, 2001.

Nelson, D. M., Tréguer, P., Brzezinski, M. A., Leynaert, A., and Quéguiner, B.: Production and dissolution of biogenic silica in the ocean: revised global estimates, comparison with regional data and relationship to biogenic sedimentation, Global Biogeochemical Cycles, 9, 359–372, 1995.

10   Pagani, M., Zachos, J. C., Freeman, K. H., Tipple, B., and Bohaty, S.: Marked decline in atmospheric carbon dioxide concentrations during the Paleogene, Science, 309, 600–603, 2005.

Peucker-Ehrenbrink, B., Ravizza, G., and Hofmann, A.: The marine $^{187}Os/^{188}Os$ record of the past 80 million years, Earth and Planetary Science Letters, 130, 155–167, 1995.

Pollock, D. E.: The role of diatoms, dissolved silicate and Antarctic glaciation in glacial/interglacial climatic change: a hypothesis, Global
15   and Planetary Change, 14, 113–125, 1997.

R Core Team: R: A language and environment for statistical computing. Version 3.2.3, R Foundation for Statistical Computing, Vienna, Austria, 2015.

Ragueneau, O., Tréguer, P., Leynaert, A., Anderson, R., Brzezinski, M., DeMaster, D. J., Dugdale, R., Dymond, J., Fischer, G., Francois, R., Heinze, C., Maier-Reimer, E., Martin-Jézéquel, E., Nelson, D., and Quéguiner, B.: A review of the Si cycle in the modern ocean: recent
20   progress and missing gaps in the application of biogenic opal as a paleoproductivity proxy, Global and Planetary Change, 26, 317–365, 2000.

Ragueneau, O., Schultes, S., Bidle, K., Claquin, P., and Moriceau, B.: Si and C interactions in the world ocean: Importance of ecological processes and implications for the role of diatoms in the biological pump, Global Biogeochemical Cycles, 20, 2006.

Ravizza, G. and Zachos, J.: Records of Cenozoic Ocean Chemistry, in: The oceans and marine geochemistry, edited by Holland, H. D. and
25   Turekian, K. K., vol. 6 of *Treatise on Geochemistry*, pp. 551 – 581, Pergamon, Oxford, 2003.

Raymo, M. and Ruddiman, W. F.: Tectonic forcing of late Cenozoic climate, Nature, 359, 117–122, 1992.

Renaudie, J. and Lazarus, D. B.: On the accuracy of paleodiversity reconstructions: a case study in Antarctic Neogene radiolarians, Paleobiology, 39, 491–509, 2013.

Salamy, K. A. and Zachos, J. C.: Latest Eocene–Early Oligocene climate change and Southern Ocean fertility: inferences from sediment
30   accumulation and stable isotope data, Palaeogeography, Palaeoclimatology, Palaeoecology, 145, 61–77, 1999.

Siever, R.: The silica budget in the sedimentary cycle, American Mineralogist, 42, 821–841, 1957.

Smetacek, V.: Diatoms and the ocean carbon cycle, Protist, 150, 25–32, 1999.

Spearman, C.: The proof and measurement of association between two things, American Journal of Psychology, 15, 72–101, 1904.

Tréguer, P. and Pondaven, P.: Silica control of carbon dioxide, Nature, 406, 358–359, 2000.

35   Tréguer, P., Nelson, D. M., Van Bennekom, A. J., DeMaster, D. J., Leynaert, A., and Quéguiner, B.: The silica balance in the world ocean: a reestimate, Science, 268, 375–379, 1995.

Tréguer, P. J. and De La Rocha, C. L.: The world ocean silica cycle, Annual review of marine science, 5, 477–501, 2013.

Tukey, J. W.: Exploratory data analysis, Addison-Wesley, Reading, MA, 1977.

Van Andel, T. H.: Mesozoic/Cenozoic calcite compensation depth and the global distribution of calcareous sediments, Earth and Planetary Science Letters, 26, 187–194, 1975.

Willey, J. D.: The effect of pressure on the solubility of amorphous silica in seawater at $0°C$, Marine Chemistry, 2, 239–250, 1974.

Wollast, R.: The Silica Problem, in: Marine Chemistry, edited by Goldberg, E. D., vol. 5 of *The Sea*, pp. 359–393, John Wiley & Sons, New York, 1974.

Yool, A. and Tyrrell, T.: Role of diatoms in regulating the ocean's silicon cycle, Global Biogeochemical Cycles, 17, 2003.

Zachos, J., Pagani, M., Sloan, L., Thomas, E., and Billups, K.: Trends, rhythms, and aberrations in global climate 65 Ma to present, Science, 292, 686–693, 2001.

Zachos, J. C., Opdyke, B. N., Quinn, T. M., Jones, C. E., and Halliday, A. N.: Early cenozoic glaciation, antarctic weathering, and seawater $^{87}Sr/^{86}Sr$: is there a link?, Chemical Geology, 161, 165–180, 1999.

Zachos, J. C., Dickens, G. R., and Zeebe, R. E.: An early Cenozoic perspective on greenhouse warming and carbon-cycle dynamics, Nature, 451, 279–283, 2008.
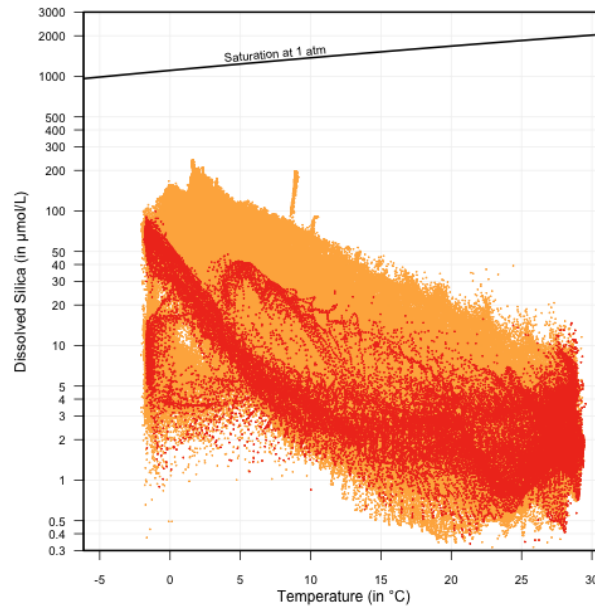
**Figure 1.** Dissolved silica is undersaturated at all depths. Saturation concentration vis-à-vis amorphous silica at 1 atm of pressure follows Wollast (1974). It is known to increase with pressure/depth (e. g. Willey, 1974). Red dots corresponds to measurements of dissolved silica (silicic acid) at the surface of the ocean and orange dots at various depths. Both corresponds to the complete World Ocean Atlas 2009 dataset (Garcia et al., 2010).
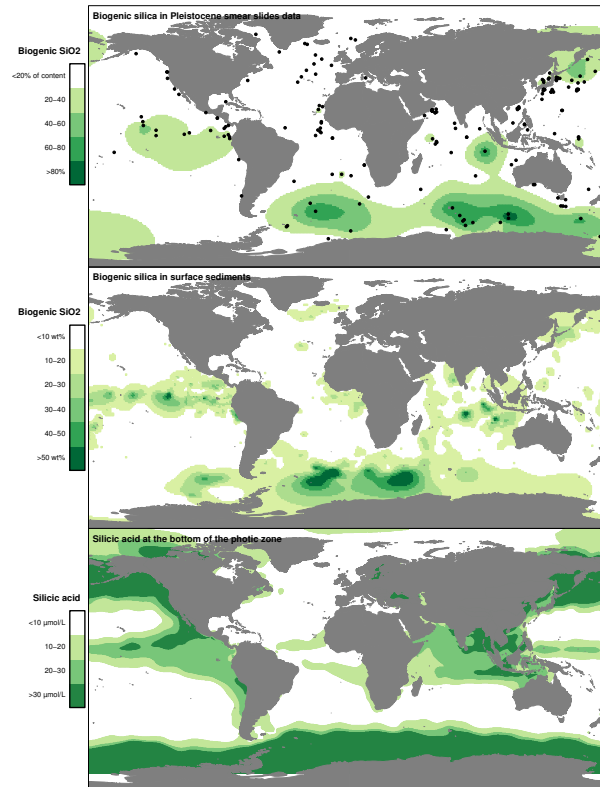
**Figure 2.** Comparison between smear slides-based data and reference data. Upper panel: cumulated distribution of diatoms, radiolarians, silicoflagellates and sponge spicules in the Pleistocene. Black dots are the siliceous microfossil-bearing sites present in the Pleistocene. Middle panel: biogenic opal in surface sediments from Archer (1996). Lower panel: silicic acid at 200m below the ocean's surface (lower limit of the euphotic zone) from Garcia et al. (2010).
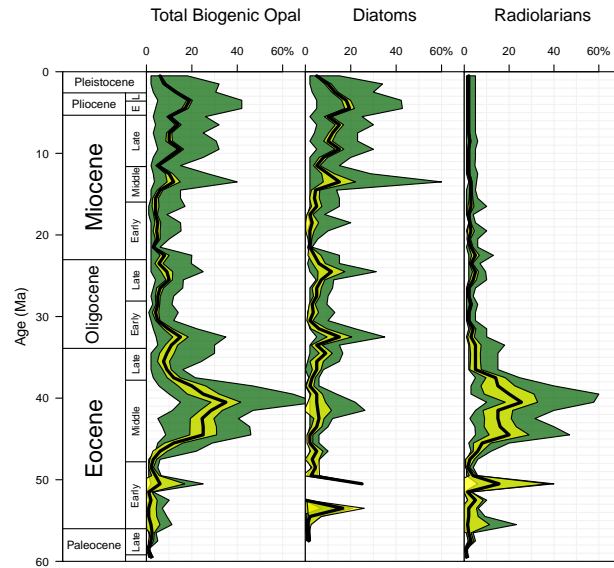
**Figure 3.** History of biogenic opal deposition. Left panel: total biogenic opal in DSDP-ODP smear slides (diatoms, radiolarians, silicoflagellates and sponge spicules combined). Middle panel: global abundance of diatoms. Right panel: global abundance of radiolarians. Bold black line is the median value in each 1 Myr time-bin while the yellow envelope delimits the 95% confidence interval on the median and the green enveloppe the interquartile range of the data.
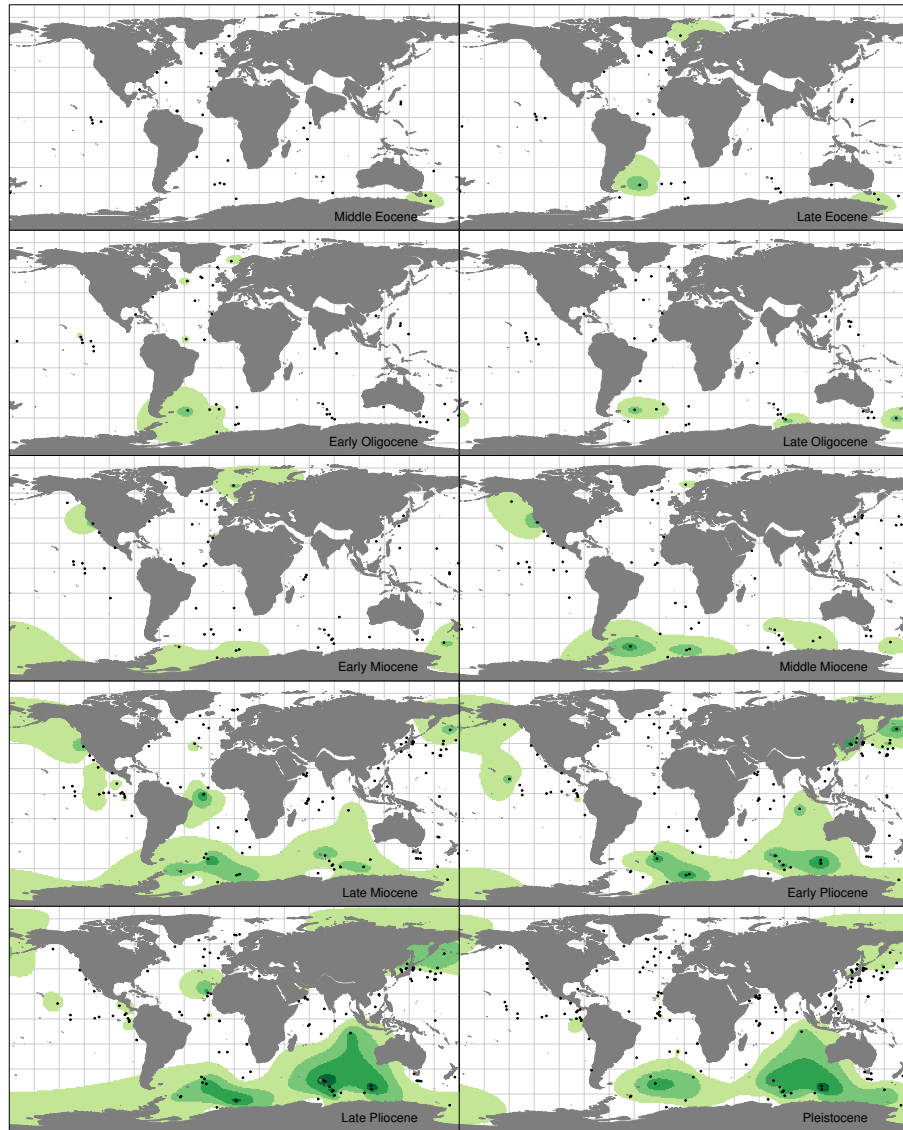
**Figure 4.** Maps of diatom abundance in DSDP-ODP smear slides during the Cenozoic. Black dots are the diatom-bearing sites present in the concerned sub-epoch. From white to dark green, the categories corresponds to: less than 20%, 20 to 40%, 40 to 60%, 60 to 80%, more than 80% (see Fig. 2 for color scale). Diatom abundance is interpolated using ordinary kriging based on an exponential model. Paleogeography from Müller et al. (2008).
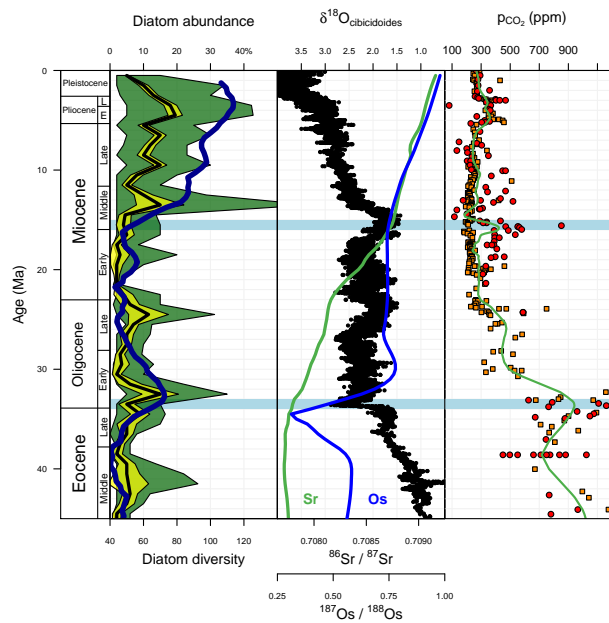
**Figure 5.** Comparison with climate and oceanography proxies. First panel – diatoms. Bold blue line is the diatom diversity from Lazarus et al. (2014). Diatom abundance as in Fig. 3. Second panel – benthic $\delta^{18}O$ (black) from Zachos et al. (2008), LOESS regression curve (Cleveland et al., 1992) of strontium (green) and osmium (blue) isotope data based on compilation by Ravizza and Zachos (2003). Third panel – Cenozoic $p_{CO_2}$ reconstruction. Orange squares (phytoplankton-based proxy) and red dots (other proxies) from Beerling and Royer (2011). Green line is a LOESS regression curve of this data.